Biological Psychiatry

Archival Report

Deficits in Neurite Density Underlie White Matter Structure Abnormalities in First-Episode Psychosis

Charlotte L. Rae, Geoff Davies, Sarah N. Garfinkel, Matt C. Gabel, Nicholas G. Dowell, Mara Cercignani, Anil K. Seth, Kathryn E. Greenwood, Nick Medford, and Hugo D. Critchley

ABSTRACT

BACKGROUND: Structural abnormalities across multiple white matter tracts are recognized in people with early psychosis, consistent with dysconnectivity as a neuropathological account of symptom expression. We applied advanced neuroimaging techniques to characterize microstructural white matter abnormalities for a deeper understanding of the developmental etiology of psychosis.

METHODS: Thirty-five first-episode psychosis patients, and 19 healthy controls, participated in a quantitative neuroimaging study using neurite orientation dispersion and density imaging, a multishell diffusion-weighted magnetic resonance imaging technique that distinguishes white matter fiber arrangement and geometry from changes in neurite density. Fractional anisotropy (FA) and mean diffusivity images were also derived. Tract-based spatial statistics compared white matter structure between patients and control subjects and tested associations with age, symptom severity, and medication.

RESULTS: Patients with first-episode psychosis had lower regional FA in multiple commissural, corticospinal, and association tracts. These abnormalities predominantly colocalized with regions of reduced neurite density, rather than aberrant fiber bundle arrangement (orientation dispersion index). There was no direct relationship with active symptoms. FA decreased and orientation dispersion index increased with age in patients, but not control subjects, suggesting accelerated effects of white matter geometry change.

CONCLUSIONS: Deficits in neurite density appear fundamental to abnormalities in white matter integrity in early psychosis. In the first application of neurite orientation dispersion and density imaging in psychosis, we found that processes compromising axonal fiber number, density, and myelination, rather than processes leading to spatial disruption of fiber organization, are implicated in the etiology of psychosis. This accords with a neurodevelopmental origin of aberrant brain-wide structural connectivity predisposing individuals to psychosis.

Keywords: Diffusion MRI, First-episode psychosis, Fractional anisotropy, Neurite density, Neurite orientation dispersion and density imaging (NODDI), White matter microstructure

http://dx.doi.org/10.1016/j.biopsych.2017.02.008

Schizophrenia and related psychoses encompass a constellation of perceptual, cognitive, and affective symptoms with characteristic expression and maturational trajectories (1). Neuroimaging and pathological studies of patients and at-risk individuals indicate distributed neurobiological brain abnormalities (2–5). Psychosis has been considered a cardinal disorder of dysconnectivity (6), in which dysfunctional integration of mental processes arises from impaired functional neural communication. Correspondingly, structural abnormalities in white matter tracts across the brain are observed in post-mortem studies (7) and in vivo noninvasive imaging using diffusion-weighted magnetic resonance imaging (MRI) (2,8,9). It is likely that white matter changes are present even before the experience of active symptoms at the onset of first-episode psychosis (FEP), preceding pharmacological treatment with neuroleptic medications (2,3,10).

The white matter abnormalities reported in FEP affect multiple fiber bundles, including interhemispheric connections, corticospinal projections, and long-range association tracts (2,11). These structural changes are associated with dysfunctional interactions between brain regions (12) and predict symptom severity in FEP (13). Moreover, neuroimaging indices of white matter integrity predict longer term outcomes, including response to treatment (2,14). White matter structural abnormalities may thus underpin early psychosis.

In vivo, white matter structure can be assessed using diffusion tensor imaging (DTI) (15). Quantitative DTI indices, including fractional anisotropy (FA) and mean diffusivity (MD), reflect microstructural features, including myelination, axonal packing density and diameter, astrocytic morphology, and angiogenesis (16,17). Genetic susceptibility to psychosis is linked to neurodevelopmental disruption of myelination, axonal guidance, and neuronal

SEE COMMENTARY ON PAGE 700

migration (18,19). Disordered axonal structure and fiber organization can result from such disruption. Thus, a key objective for understanding the nature, etiology, and implications of white matter abnormalities in FEP is to characterize microstructural differences in axonal structure, including axonal number, packing density, and myelination, and to differentiate these from variations in fiber geometry.

However, conventional DTI analyses model a single water compartment within each voxel. Thus, FA and MD measures cannot distinguish specific fine-grained contributions to white matter structure, as indices estimated from a standard tensor model include contributions from both neurite density (ND) and fiber arrangement. More advanced analytic approaches can now model intracellular and extracellular water diffusion separately, enabling a more detailed description of white matter structure (20,21). Neurite orientation dispersion and density imaging (NODDI) applies a multicompartment model to separate contributions of neurite density and fiber orientation (Figure 1). Approaches such as NODDI benefit from long MRI acquisition times; however, newer clinically feasible protocols have been developed (21). These permit detailed characterization of white matter integrity that can shed light on the etiology of brain disorders and provide indicators for diagnosis, treatment response, and prognosis (14,22,23).

In this study of patients with FEP, we applied the NODDI technique (21) to distinguish changes in axonal microstructure from changes in fiber geometry. This enables deeper characterization of white matter abnormalities than is possible with indices such as FA and MD. We hypothesized that specific NODDI signatures of microstructural integrity indicate the presence of a pathoetiological process of likely neurodevelopmental origin that underpins abnormalities across multiple white matter tracts at an early stage of illness. Ultimately, we seek mechanistic knowledge with clinical utility for biomarking and for developing new preventive interventions.

METHODS AND MATERIALS

Participants

Patients with FEP were recruited from the Sussex Partnership National Health Service Trust Early Intervention in Psychosis service (n = 35; 27 men, 8 women; mean age, 26.9 years; age range, 19–39 years; mean years of education, 13.4 years). The majority of patients (66%; 23 of 35) were 18–30 years old, and 34% (12 of 35) were 30–39 years old, suggesting heterogeneity within the FEP population (e.g., schizophrenia and affective psychosis). Diagnosis of psychotic episode was made by a U.K. psychiatrist. At the time of MRI, each patient remained under clinical care of the Early Intervention in Psychosis service. Control participants, matched for age, gender, and years of education, with no history of psychiatric or neurological disorder, were recruited via advertisement within the local community (n = 19; 13 men, 6 women; mean age, 24.7 years; age range, 18–38 years; mean years of education, 13.8 years). All participants gave written informed consent. The study was approved by the National Research Ethics Service Camden and Islington Research Ethics Committee.

Clinical Assessments and Medication

On the day of MRI, symptom severity was assessed using the Positive and Negative Syndrome Scale short form (PANSS-S) (24) by a trained assessor (GD). We recorded any psychoactive medication and calculated olanzapine dose-equivalents (25). Of the patients, 11 were taking only antipsychotic medications, 7 were taking antipsychotics and additional psychoactive medications (e.g., serotonin reuptake inhibitors), 4 were taking psychoactive medications but no antipsychotics, and 13 were unmedicated, reflecting typical heterogeneity of early interventions within an FEP service (Table 1; see Supplemental Table S1 for individual patient data, including duration of medication, onset of symptoms to MRI, and diagnosis).

Medication and Symptom Severity

We tested for a relationship between medication and symptom severity (PANSS-S) using multiple regression in SPSS version 22 (IBM Corp., Armonk, NY) with olanzapine dose-equivalent as a dependent variable and PANSS positive, negative, and cognitive disorganization scores as independent variables.

Diffusion MRI Data Acquisition

MRI data were acquired on a 1.5T MAGNETOM Avanto MRI scanner (Siemens Healthcare GmbH, Erlangen, Germany). Multishell diffusion-weighted data were acquired with single-shot, twice-refocused pulse gradient spin-echo echo planar imaging (voxel size 2.5 × 2.5 × 2.5 mm^3, 60 axial slices, matrix size 96 × 96, field of view 240 × 240 mm^2, repetition time = 8400 ms, echo time = 99 ms). Three b-value shells were acquired (9 directions with b = 300 s/mm^2, 30 directions with b = 800 s/mm^2, and 60 directions with b = 2400 s/mm^2), optimized for NODDI (21). Eleven images with no diffusion weighting (b ≈ 0 s/mm^2) were acquired. Total acquisition time was 17 minutes.

Diffusion MRI Analysis

Data were processed and analyzed using FSL (version 5.0.7; http://fsl.fmrib.ox.ac.uk/fsl/fslwiki/), DTI-TK (version 2.3.1; http://dti-tk.sourceforge.net/pmwiki/pmwiki.php), and in-house scripts with the NODDI MATLAB toolbox (The MathWorks, Inc., Natick, MA; http://mig.cs.ucl.ac.uk/index.php?n=Tutorial.NODDImatlab) (21). DICOM images were converted to NIfTI images using mcverter (https://lcni.uoregon.edu/downloads/mriconvert/mriconvert-and-mcverter).

We computed head movement using FSL eddy_correct to obtain motion indices in three translations (eddy_correct output logs). The root mean square of total motion was calculated, summing total displacement (26). A between-subjects t test (SPSS version 22) indicated that as a group, patients did not move significantly more than control subjects (mean FEP displacement 57 mm, SD 11 mm; control 52 mm, SD 11 mm: $t_{52} = -1.749$, $p = .086$). However, individual differences in head movement can nevertheless contribute to estimations of diffusion indices (27). We therefore included a motion covariate in all statistical tests (see below).

To correct for motion and eddy currents, we implemented a multistep image registration using FLIRT in FSL. Image

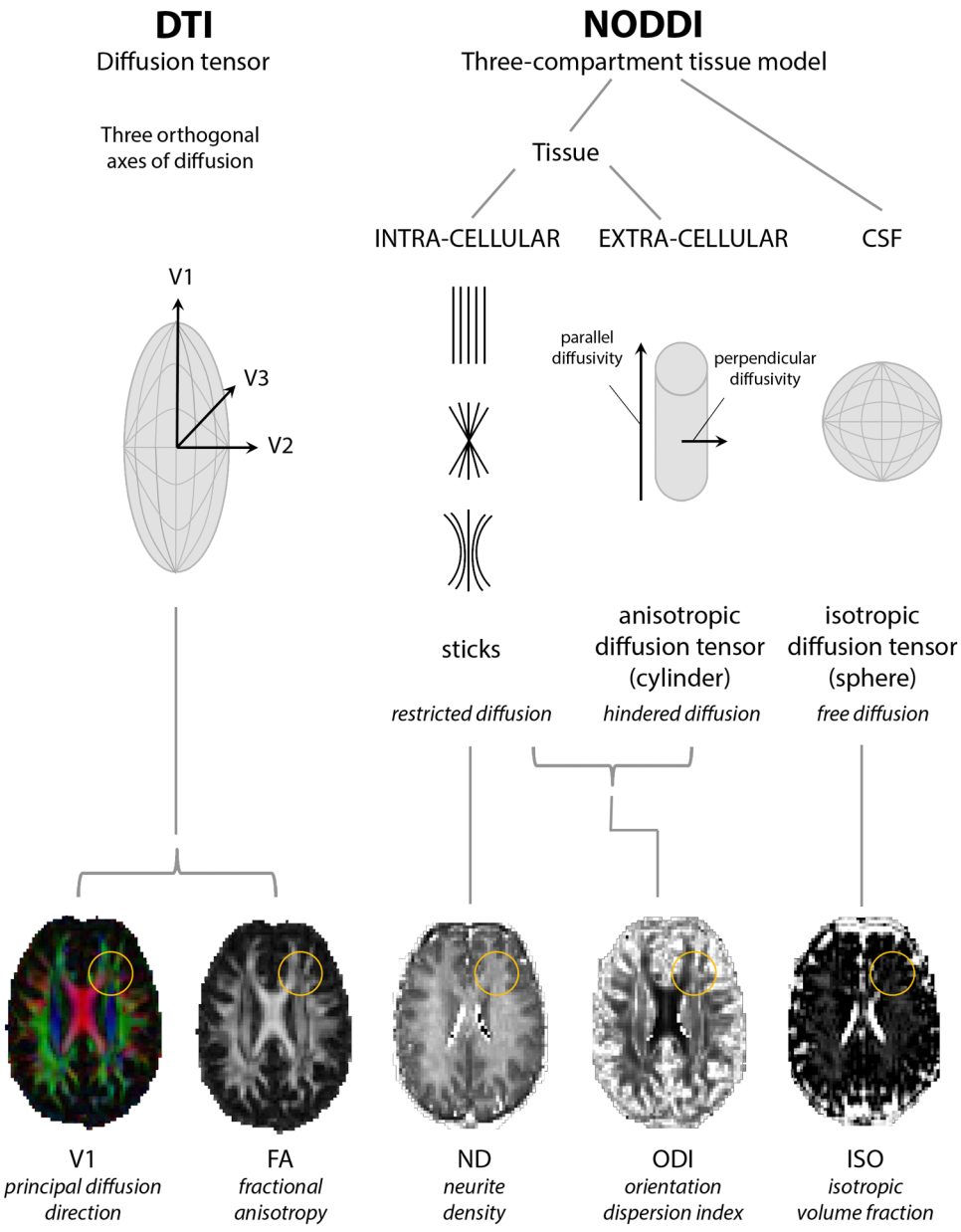

Figure 1. The neurite orientation dispersion and density imaging (NODDI) technique and how it differs from traditional diffusion tensor imaging (DTI). In DTI, a diffusion tensor models three orthogonal axes of diffusion (V1, V2, V3), from which fractional anisotropy (FA) and mean diffusivity (MD) can be estimated. NODDI models diffusion according to three compartments: restricted diffusion in the intracellular compartment, hindered diffusion in the extracellular compartment, and free diffusion in cerebrospinal fluid (CSF). From this model, parameter maps representing neurite density (ND) and orientation dispersion index (ODI) can be estimated. Yellow circles highlight a region where changes in FA can be accompanied by changes in both ND and ODI.

contrast in diffusion-weighted imaging is strongly dependent on b-value. It was therefore not possible to reliably coregister all diffusion-weighted volumes to the same target image. Instead, a stepwise registration process was adopted. First, a mean image was generated for each shell (b = 0, 300, 800, 2400 s/mm^2) by averaging the volumes for each diffusion direction in the corresponding shell. Next, a transformation matrix was computed to coregister each individual volume with the mean image for the corresponding shell. Another transformation matrix was computed to coregister the b = 300, 800, and 2400 s/mm^2 mean images with the mean b = 0 image. Finally, the required transformation matrices were combined to transform each individual volume into the same space as the mean b = 0 volume.

Following motion and eddy current correction, diffusion data were stripped of nonbrain tissue using BET2 in FSL, and a brain mask was derived to constrain anatomical fitting of DTI and NODDI parameters. Diffusion tensors were fitted using DTIFIT in FSL, providing output maps of the three diffusion tensor eigenvectors (ε_1–ε_3) and eigenvalues (λ_1–λ_3), FA, and MD. NODDI models diffusion according to three tissue compartments: intracellular restricted diffusion, modeled by sticks; extracellular hindered diffusion, modeled by parallel and perpendicular diffusion in an anisotropic tensor; and cerebrospinal fluid free diffusion, modeled by an isotropic tensor (Figure 1). The restricted diffusion of the intracellular component gives rise to intracellular volume fraction maps, which index neurite density, whereas both restricted and hindered

Table 1. Participant Demographics, Patient PANSS-S Scores, Olanzapine Dose-Equivalents, Duration of Medication, and Time From Onset of Symptoms to MRI

	FEP (n = 35)	CON (n = 19)	Group Difference Statistical p Value
Male/Female, n	27/8	13/6	.37[a]
Age, Years	26.89 (19–39)	24.68 (18–38)	.19[b]
Years of Education	13.37 (11–17)	13.84 (11–17)	.34[b]
PANSS-S: Positive	5.40 (3–10)	—	—
PANSS-S: Negative	5.29 (3–12)	—	—
PANSS-S: Cognitive Disorganization	3.09 (2–6)	—	—
Olanzapine Dose-Equivalent, mg	13.65 (3.7–30)	—	—
Duration of Medication, Days	479 (36–1328)	—	—
Time From Onset to MRI, Days	667 (39–1447)	—	—

Mean olanzapine dose-equivalent and duration of medication given according to the average of the 18 medicated patients. Olanzapine dose-equivalents calculated according to criteria in Leucht *et al.* (25). Values are given as mean (range) except where noted.

CON, control subjects; FEP, patients with first-episode psychosis; MRI, magnetic resonance imaging; PANSS-S, Positive and Negative Syndrome Scale short form.

[a] χ^2 test.

[b] t test.

diffusion of the intracellular and extracellular components give rise to orientation dispersion index (ODI) maps, which index fiber arrangement. The NODDI WatsonSHStickTortIsoV_B0 model (21) was applied, providing output maps of neurite ODI (indexing fiber arrangement), and intracellular volume fraction (indexing ND).

To compare DTI indices between patients and control subjects, we used tract-based spatial statistics (TBSS) (28) in FSL, with DTI-TK tensor-based registration, in a hybrid DTI-TK–TBSS pipeline. DTI-TK uses the full tensor for registration, rather than FA only (29). This improves registration accuracy compared with conventional TBSS registration using FA (30). A tensor image was created for each participant by converting diffusion eigenvectors and eigenvalues with fsl_to_dtitk in DTI-TK. A study-specific population template was created from participants' tensor images, by iterative affine, then diffeomorphic, registration to the group mean. This population template was registered to the Illinois Institute of Technology IITmean_tensor.nii mean tensor template (version 4.1; https://www.nitrc.org/projects/iit/), in Montreal Neurological Institute space, to create the final study template. These two stages generated matrices of transformations from each individual's native space to the population template, then to standard space. These matrices were used to calculate a deformation field capturing transformations from native to standard space in one interpolation for each participant [see (31,32)].

Following tensor-based registration, in DTI-TK a mean FA map was calculated from the final tensor template. This was skeletonized using tbss_skeleton in FSL to create a mean FA skeleton. Individual participants' FA maps were calculated in DTI-TK from standard-space registered tensor images and merged into a 4D file of all participants' FA maps for entering to TBSS. FA maps were then projected onto the mean FA skeleton using tbss_4_prestats with a threshold of FA >0.3.

Deformation fields, capturing transformations from native to standard space, were applied to each participant's MD, ODI, and ND images to test for group differences in MD and NODDI indices. The skeleton distance maps calculated for the FA images in tbss_4_prestats were then applied to the MD, ODI, and ND images using tbss_skeleton in FSL to project the non-FA images onto the mean FA skeleton [see (33)].

Voxelwise Statistics

Voxelwise statistics were carried out using PALM in FSL (34). Four design matrices tested: 1) group difference, with images categorized as "patient" or "control"; 2) group difference, with age covariates entered separately for patients and control subjects; 3) correlation with olanzapine dose-equivalent in the patient group only; and 4) correlation with the positive, negative, and cognitive disorganization scores of the PANSS-S, including olanzapine dose-equivalent as a covariate, in the patient group only. The high correlation between the PANSS-S subscales, indicating shared variance (see Results), necessitated the use of three different design matrices for "positive," "negative," and "cognitive disorganization" scores.

Age, gender, and total head movement were entered as nuisance covariates in each design matrix. All covariates were mean-centered across participants. These design matrices were applied to the FA, MD, ODI, and ND images using PALM with 10,000 permutations, tail acceleration (35), and threshold-free cluster enhancement (36). The option "-corrcon" was applied to correct for multiple contrast testing (35). Statistical images were thresholded at $p < .05$ with familywise error correction for multiple voxel comparisons. Significant voxels were ascribed anatomical labels using atlasquery in FSL with the Johns Hopkins University ICBM-DTI-81 White Matter Labels and Johns Hopkins University White Matter Tractography atlases and a minimum likelihood of at least 0.1% (Table 2). To test for overlap between significant voxels in different contrasts (Figure 2E and Supplemental Figure S1), statistical images were thresholded at $p < .05$ familywise error, binarized, summed, and the resulting image thresholded at a voxel value of k, where k = number of input statistical images (i.e., testing for voxels present in all k original contrasts at $p < .05$ familywise error).

Region of Interest Comparison

We extracted the mean FA, MD, ODI, and ND for control subjects and patients with FEP in the corpus callosum body (Johns Hopkins University ICBM-DTI-81 atlas), masking the region of interest by the mean_FA_skeleton_mask to include only skeleton voxels (Supplemental Figure S2).

RESULTS

Medication and Symptom Severity

Multiple regression revealed no simple relationship between olanzapine dose-equivalent and symptom severity on the three PANSS-S subscales ($F_3 = 0.21$, $p = .891$). Nevertheless, PANSS-S scores correlated with each other: positive symptoms with negative symptoms ($r = .35$, $p = .020$), positive

Table 2. Anatomical Labels of Significant Voxels[a] According to Johns Hopkins University ICBM-DTI-81 White Matter Labels and Johns Hopkins University White Matter Tractography Atlases in FSL

	Group Difference					Age (FEP and CON)				Age (FEP)				Olanzapine Dose-Equivalent			
Tract	FA	MD	ODI	ND	FA+ ND	FA	MD	ODI	ND	FA	MD	ODI	ND	FA	MD	ODI	ND
Corpus Callosum (Genu)	B	B		B	B			B		B		B					
Corpus Callosum (Body)	B	B		B	B			B		B				B			
Corpus Callosum (Splenium)	B			B	B									B			
Forceps Major	B	B		B	B												
Forceps Minor	B	B		B	B			B		B		B		B			
Fornix (Column and Body)																	
Fornix (Cres)	L																
Internal Capsule (Anterior)		R		R										R			
Internal Capsule (Posterior)		B		B	L												
Internal Capsule (Retrolenticular Part)	L	B		B	L									L			
External Capsule	L	B		L	L									R			
Corona Radiata (Anterior)	B	B		B	B					B				B			
Corona Radiata (Superior)	B	B		B	B									R			
Corona Radiata (Posterior)	B	B		B	B									R			
Anterior Thalamic Radiation	L	B		B	L					B				B			
Posterior Thalamic Radiation	B	B		B	B												
Corticospinal Tract	B	B		B	B									R			
Cingulum (Cingulate Gyrus)	L							B		B		B		R			
Cingulum (Hippocampus)																	
Inferior Fronto-occipital Fasciculus	B	B		B	B					B				B			
Inferior Longitudinal Fasciculus	B	B		B	B												
Superior Longitudinal Fasciculus	B	B		B	B									B			
Uncinate Fasciculus	L	B		B	L					B				B			

B, bilateral; CON, control subjects; FEP, patients with first-episode psychosis; FA, fractional anisotropy; L, left hemisphere; MD, mean diffusivity; ND, neurite density; ODI, orientation dispersion index; R, right hemisphere.

[a]$p < .05$ familywise error with threshold-free cluster enhancement.

symptoms with cognitive disorganization ($r = .45$, $p = .004$), and negative symptoms with cognitive disorganization ($r = .66$, $p < .001$).

Poorer White Matter Structure in FEP Indicated by Reduced ND

Patients with FEP showed abnormalities across multiple white matter tracts with lower FA and greater MD, compared with control subjects (Figure 2A and B and Table 2). NODDI analyses showed no significant group differences in ODI (Figure 2C), yet patients had lower ND (Figure 2D and Table 2). This overlapped anatomically with many regions of lower FA (Figure 2E), as well as regions of higher MD (Supplemental Figure S1). Interhemispheric connections, corticospinal projections, and association fibers showed these group differences in FA, MD, and ND (Table 2; see Supplemental Figure S2 for an example region of interest of corpus callosum skeleton voxels). These data suggest that white matter abnormalities in patients with FEP chiefly reflect reduced ND, rather than abnormalities in geometrical organization and angular variation of fibers, suggesting a distinct developmental cause (37).

ODI Correlates With Age

We tested for an association between age and white matter structure, first across all participants (FEP patients and controls). Age correlated positively with ODI in the anterior corpus callosum (Figure 3A and Table 2). This suggests that white matter structural geometry changes with increasing age (even within a relatively young adult cohort), expressed as disruption of fiber orientation (21).

We next tested for an association between age and white matter structure in patients with FEP and in control subjects separately and examined age-by-group interactions to evaluate whether age-related changes in ODI were accelerated in patients with FEP. In control subjects, there were no significant correlations with age. In patients with FEP, however, age correlated negatively with FA in the corpus callosum and association fibers (Figure 3B and Table 2) and positively with ODI in the anterior corpus callosum (Figure 3C and Table 2). The age-by-group interactions for FA and ODI were below threshold significance.

Impact of Medication

Within the patient group, we tested for associations between medication and white matter structure, using correlations of olanzapine dose-equivalent with FA, MD, ODI, and ND. Olanzapine dose-equivalent correlated negatively with FA (Figure 4) within specific white matter tracts, linking higher medication dose to poorer white matter structure (Table 2). There were no significant correlations with MD, ODI, or ND.

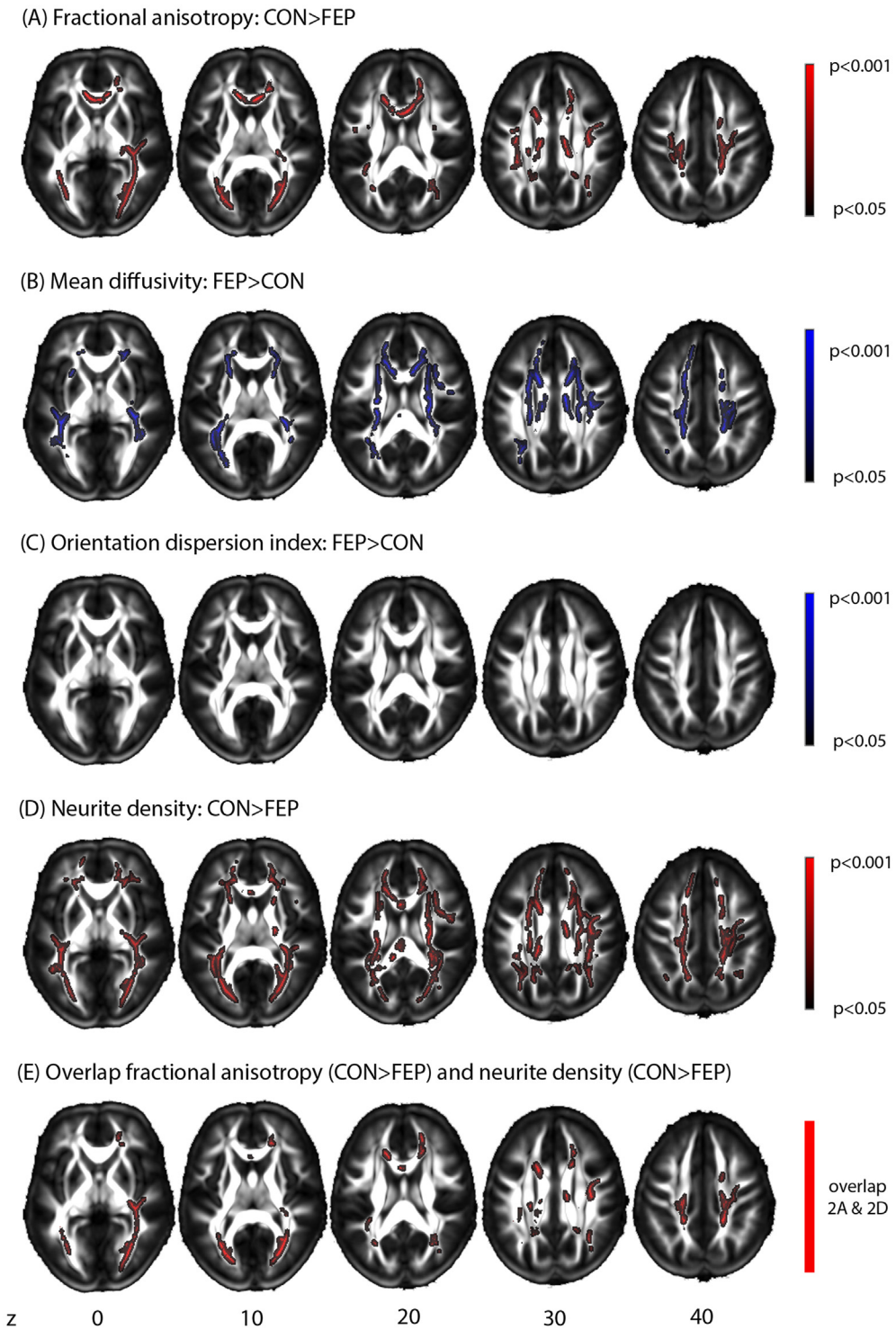

Figure 2. Group difference between patients with first-episode psychosis (FEP) and control subjects (CON). **(A)** Reduced fractional anisotropy. **(B)** Increased mean diffusivity. **(C)** No significant group differences in orientation dispersion index. **(D)** Reduced neurite density. **(E)** Overlapping voxels of reduced fractional anisotropy and reduced neurite density. **(A–D)** Tracts shown at $p < .05$ familywise error with threshold-free cluster enhancement. Tracts with bilateral white matter abnormalities shown here include the corpus callosum, corticospinal tract, anterior thalamic radiation, inferior fronto-occipital fasciculus, superior longitudinal fasciculus, and inferior longitudinal fasciculus (also see Table 2). Slice labels (0–40) indicate *z* coordinate in Montreal Neurological Institute space.

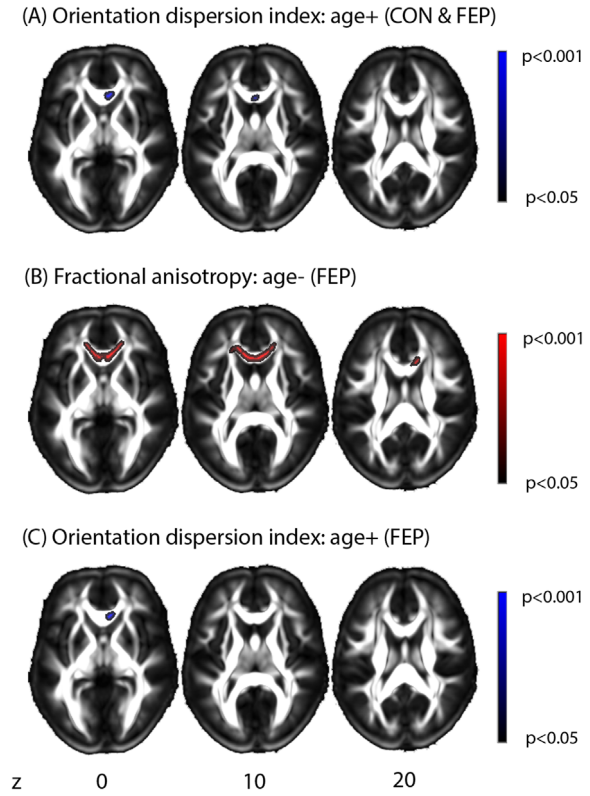

Figure 3. Age and white matter structure. **(A)** Positive correlation with orientation dispersion index in both patients with first-episode psychosis (FEP) and control subjects (CON) in the anterior corpus callosum. **(B)** Negative correlation with fractional anisotropy in FEP only. **(C)** Positive correlation with orientation dispersion index in FEP only. **(A–C)** Tracts shown at $p < .05$ familywise error with threshold-free cluster enhancement. Slice labels (0–20) indicate z coordinate in Montreal Neurological Institute space.

PANSS-S Scores

We observed no suprathreshold correlations between PANSS-S positive, negative, and cognitive disorganization scores with FA, MD, ODI, or ND.

DISCUSSION

We found anatomically widespread white matter structure alterations in patients with FEP. Using diffusion imaging combined with NODDI analysis, we demonstrated these white matter alterations as primarily reflecting reduced ND. This observation can be attributed to specific changes that include lower axonal count, reduced packing density, and lower myelination (21). Thus, we provide an important first demonstration that white matter disturbance in FEP is driven by these microstructural features rather than fiber orientation, which standard diffusion tensor–derived parameters, notably FA, cannot distinguish. In patients, age impacted fiber geometry: fiber orientation dispersion increased with age, an effect not present in the control subjects. Together these findings provide fresh insight into the nature of the biological disruption underpinning white matter abnormalities in psychosis.

Our findings have implications for understanding psychosis as a neurodevelopmental dysconnectivity syndrome. They highlight the value of fine-grained characterization of white matter abnormalities, including ND, to yield insights into pathoetiological mechanisms that can determine patients' long-term prognosis and response to treatment.

Psychosis as a Neurodevelopmental Dysconnectivity Risk Syndrome

Disrupted white matter structure is likely to precede the onset of FEP (2). In adolescent cohorts within the general population, alterations in white matter structure associated with a psychotic experience can be observed before diagnosis of a mental health condition (3,10). This suggests that an aberrant neurodevelopmental risk state, centered on a structural vulnerability that compromises functional connectivity, can predispose to psychotic symptoms, which in some individuals may progress to a diagnosed disorder.

To better understand the origins of structural dysconnectivity in psychosis, we sought a more detailed characterization of the microstructural abnormalities that underpin white matter differences (notably, in FA and MD) previously reported using diffusion MRI (2,8). Using the NODDI technique, we modeled intracellular and extracellular contributions to diffusion. This permitted us to differentiate changes to ND versus fiber orientation. Our in vivo observation of reduced ND might arise from alterations in developmental processes, such as neuronal migration, axon guidance, myelination, and synaptic pruning (18,19,38). For example, aberrant neuronal migration may reduce the number of neurites within a fiber bundle, whereas excessive synaptic pruning may lead to withdrawal of axonal projections.

It is noteworthy that we did not observe significant group differences in neurite orientation dispersion except in regard to age. Developmental insults can theoretically affect neurite orientation, e.g., through disruption of brain matrix and/or programmed migration path. However, this does not reliably determine risk of early psychosis. Nevertheless, alterations in fiber arrangement can still foster processes that lead to secondary (age-related) organizational disruption. In the general population, while ND increases logarithmically throughout adolescent life, the ODI decreases exponentially from early adulthood into later life (37,39). In light of this, our results suggest a core deficit in ND during early development in individuals with psychosis, yet the experience of a psychotic episode may encourage premature age-related changes in white matter geometry, reflected by increasing fiber orientation dispersion with age. Future imaging studies of at-risk populations should usefully integrate genotyping of specific polymorphisms linked to neuronal development, with estimation of NODDI parameters from diffusion MRI and nonlinear modeling of relevant demographic features to gain more precise insight into the developmental origins and biological nature of microscale disruptions in white matter relevant to psychosis.

Distribution of Network Abnormalities

We observed reductions in white matter FA and ND within all lobes, affecting interhemispheric, corticospinal, and association tracts. Our findings are inconsistent with focal concentration of structural dysconnectivity in frontal and temporal lobes (8) and fit with the observed broader distribution of white matter changes across multiple regions in psychosis (2,9). This widespread

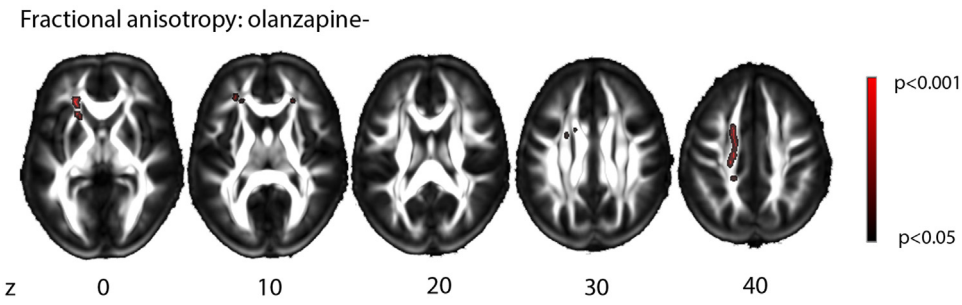

Figure 4. Medication level (olanzapine dose-equivalent) and white matter structure. Negative correlation with fractional anisotropy ($p < .05$ familywise error with threshold-free cluster enhancement) in the internal capsule, corticospinal tract, anterior thalamic radiation, inferior fronto-occipital fasciculus, and superior longitudinal fasciculus (also see Table 2). Slice labels (0–40) indicate *z* coordinate in Montreal Neurological Institute space.

expression of structural connectivity abnormalities suggests a shared, and perhaps early, etiology that accords with the diverse expression of symptoms, including alterations to conscious experience, in psychosis. Moreover, the structural connectivity abnormalities likely underpin concomitant dysfunctional network interactions observed in functional MRI (10,12,40), which can reflect symptom experience, severity of psychosis, and response to treatment (2,13,41).

In the context of predictive coding accounts of psychosis (42–44), these widespread reductions in ND may result in network-wide failures to balance ascending sensory "prediction error" signals against descending top-down perceptual predictions (45). These failures may arise from a reduced capacity to modulate synaptic gain, as a result of reduced efficiency of impoverished modulatory axonal projections.

Disorder Severity and Interaction With Medication

We found that in a subset of white matter tracts, FA was associated with neuroleptic dose level. The question arises as to whether white matter abnormalities may be more extreme in patients who require higher levels of neuroleptic therapy and/or whether such medications alter white matter.

In our sample, we did not observe significant correlations between PANSS-S scores and white matter. Previous diffusion imaging studies in FEP report correlations between white matter structure and PANSS scores (13,46). In medicated patients, drug therapy typically improves symptoms—hence the PANSS-S may not reflect severity at presentation and diagnosis, constraining the interpretation of correlations between symptom severity score and white matter structure.

Nevertheless, antipsychotics may change white matter, according to animal models (47) and human imaging (48–50). The mean duration of medication for the 18 medicated patients was more than a year, which may be sufficient time for neuroleptic-induced plasticity or changes, although there were individual patient differences. However, it is interesting that there were no effects of medication on ND or orientation dispersion, which suggests effects on FA do not relate to axonal structure or fiber geometry. At the present time, evidence for the impact of neuroleptics on white matter appears to be equivocal (2) and may index historical patterns of medication use.

To further address how antipsychotic use relates to microstructural features, longitudinal studies of larger cohorts may permit examination of subgroups of patients differentiated according to precise antipsychotic medication taken and relative expression of symptoms, alongside premedication and postmedication quantification of white matter structural integrity including NODDI measures.

Predictive Value for Prognosis and Treatment Response

White matter structure at FEP is likely to relate to long-term prognosis and response to treatment (2). It is essential that the biological nature of white matter aberration is understood if microstructural measures are to prove valuable as clinical biomarkers. The multicompartment model of the NODDI technique is particularly valuable in this regard, given that it can identify in greater detail the nature of the neuroanatomical change in white matter, beyond diffusion tensor–derived indices such as FA. Patients with reduced ND may be less likely to respond to drug therapies if a decrease of axonal bundles has already occurred, while patients may be poised to respond well if they exhibit a relative preservation of ND, whereby the function of the remaining neurons can be boosted. In following a longitudinal outcome, if ND continues to decline with repeated episodes, the potential for recovery may diminish.

Treatments typically focus on managing symptoms after they have emerged. However, prevention is an ultimate goal. Perhaps by identifying individuals most at risk for psychosis through expression of developmental dysconnectivity, interventions can be implemented before onset of psychosis. In the present study, we highlight the overarching contribution of disordered ND (rather than fiber geometry) to dysconnectivity in FEP. Effective early treatment interventions might usefully target the prevention of neurite depletion as a therapeutic target.

The identification of imaging biomarkers that can be acquired in a short acquisition time will help characterize the neurobiology of poor white matter structure and thereby inform the development of new targeted early interventions. Practically, a brief imaging protocol is necessary for patients who may have problems tolerating longer imaging times. Even if scanning is broadly tolerated, movement and other artifacts may compromise data quality. Including motion covariates remains important, as head movement impacts estimation of diffusion indices (27). It is also important to consider tradeoffs between impact of high b-values and number of directions on accuracy of tensor and other model fits (26,51). Nevertheless, a multishell diffusion acquisition with NODDI analysis offers biologically more insightful indices of white matter structure than is possible with a single shell, yet requires only a modest increase in acquisition time, particularly with simultaneous

multislice acquisition (52). NODDI thus provides a practical route to address microstructural abnormalities in investigations of white matter structure in patients with psychosis or other neuropsychiatric disorders.

Limitations

While this is the first demonstration of ND deficits in FEP, it is relevant to consider the heterogeneity of the sample, with varied diagnostic outcomes, including schizophrenia, affective psychosis, and substance-induced psychosis (Supplemental Table S1). The age distribution also reflected such heterogeneity, encompassing a period of 20 years. Larger patient samples and longitudinal studies may permit greater power and deeper insight into how NODDI indices may differ in clinical subcategories and at varying time points across the life span. Beyond NODDI analyses, a future goal of diffusion modeling is to further dissect contributions of myelination, axonal number, packing density, and diameter to ND (16,17). Multimodal functional and structural data sets can provide mechanistic insights, where multiple testing on non–normally distributed data will benefit from nonparametric approaches such as permutations tests (34).

Conclusions

NODDI separates changes in ND relating to axonal structure from alterations in fiber geometry. In FEP, ND is reduced across anatomically distributed white matter tracts and overlaps anatomically with changes in FA. This accords with evidence that psychosis is a neurodevelopmental dysconnectivity risk syndrome, in which reduced brain-wide structural connectivity and impairment of axonal structure increase the likelihood of developing abnormal conscious experiences of the self and of the world.

ACKNOWLEDGMENTS AND DISCLOSURES

This work was supported by the Dr. Mortimer and Theresa Sackler Foundation and European Research Council Advanced Grant No. 324150, Cardiac Control of Fear in the Brain (HDC and SNG).

We thank Abigail Wright for assistance with patient diagnosis records.

The authors report no biomedical financial interests or potential conflicts of interest.

ARTICLE INFORMATION

From the Sackler Centre for Consciousness Science (CLR, SNG, AKS, NM, HDC), School of Psychology (GD, KEG), and School of Engineering & Informatics (AKS), University of Sussex, Falmer, Brighton; the Division of Neuroscience (CLR, SNG, MCG, NGD, MC, NM, HDC), Brighton & Sussex Medical School, Falmer, Brighton; and Sussex Partnership National Health Service Foundation Trust (GD, KEG, NM, HDC), United Kingdom.

Address correspondence to Charlotte L. Rae, Ph.D., Clinical Imaging Sciences Centre, Brighton & Sussex Medical School, University of Sussex, Falmer, Brighton BN1 9RR, UK; E-mail: c.rae@bsms.ac.uk.

Received Aug 3, 2016; revised Jan 30, 2017; accepted Feb 10, 2017.

Supplementary material cited in this article is available online at http://dx.doi.org/10.1016/j.biopsych.2017.02.008.

REFERENCES

1. Frith C, Johnstone EC (2003): Schizophrenia: A Very Short Introduction. Oxford: Oxford University Press.
2. Canu E, Agosta F, Filippi M (2015): A selective review of structural connectivity abnormalities of schizophrenic patients at different stages of the disease. Schizophr Res 161:19–28.
3. O'Hanlon E, Leemans A, Kelleher I, Clarke MC, Roddy S, Coughlan H, *et al*. (2015): White matter differences among adolescents reporting psychotic experiences: A population-based diffusion magnetic resonance imaging study. JAMA Psychiatry 72:668–677.
4. Lawrie SM, McIntosh AM, Hall J, Owens DG, Johnstone EC (2008): Brain structure and function changes during the development of schizophrenia: The evidence from studies of subjects at increased genetic risk. Schizophr Bull 34:330–340.
5. van den Heuvel MP, Scholtens LH, de Reus MA, Kahn RS (2016): Associated microscale spine density and macroscale connectivity disruptions in schizophrenia. Biol Psychiatry 80:293–301.
6. Wernicke C (1906): Grundrisse der Psychiatrie in klinischen Vorlesungen. Leipzig: Thieme.
7. Uranova N, Orlovskaya D, Vikhreva O, Zimina I, Kolomeets N, Vostrikov V, *et al*. (2001): Electron microscopy of oligodendroglia in severe mental illness. Brain Res Bull 55:597–610.
8. Ellison-Wright I, Bullmore E (2009): Meta-analysis of diffusion tensor imaging studies in schizophrenia. Schizophr Res 108:3–10.
9. Bora E, Fornito A, Radua J, Walterfang M, Seal M, Wood SJ, *et al*. (2011): Neuroanatomical abnormalities in schizophrenia: A multimodal voxelwise meta-analysis and meta-regression analysis. Schizophr Res 127:46–57.
10. Drakesmith M, Dutt A, Fonville L, Zammit S, Reichenberg A, Evans CJ, *et al*. (2016): Mediation of developmental risk factors for psychosis by white matter microstructure in young adults with psychotic experiences. JAMA Psychiatry 73:396–406.
11. Perez-Iglesias R, Tordesillas-Gutierrez D, Barker GJ, McGuire PK, Roiz-Santianez R, Mata I, *et al*. (2010): White matter defects in first episode psychosis patients: A voxelwise analysis of diffusion tensor imaging. Neuroimage 49:199–204.
12. Benetti S, Pettersson-Yeo W, Allen P, Catani M, Williams S, Barsaglini A, *et al*. (2015): Auditory verbal hallucinations and brain dysconnectivity in the perisylvian language network: A multimodal investigation. Schizophr Bull 41:192–200.
13. Filippi M, Canu E, Gasparotti R, Agosta F, Valsecchi P, Lodoli G, *et al*. (2014): Patterns of brain structural changes in first-contact, antipsychotic drug-naive patients with schizophrenia. AJNR Am J Neuroradiol 35:30–37.
14. Pina-Camacho L, Garcia-Prieto J, Parellada M, Castro-Fornieles J, Gonzalez-Pinto AM, Bombin I, *et al*. (2015): Predictors of schizophrenia spectrum disorders in early-onset first episodes of psychosis: A support vector machine model. Eur Child Adolesc Psychiatry 24: 427–440.
15. Basser PJ, Mattiello J, LeBihan D (1994): Estimation of the effective self-diffusion tensor from the NMR spin echo. J Magn Reson 103: 247–254.
16. Wheeler-Kingshott C, Cercignani M (2009): About "axial" and "radial" diffusivities. Magn Reson Med 61:1255–1260.
17. Zatorre RJ, Fields RD, Johansen-Berg H (2012): Plasticity in gray and white: Neuroimaging changes in brain structure during learning. Nat Neurosci 15:528–536.
18. Kamiya A, Tomoda T, Chang J, Takaki M, Zhan C, Morita M, *et al*. (2006): DISC1-NDEL1/NUDEL protein interaction, an essential component for neurite outgrowth, is modulated by genetic variations of DISC1. Hum Mol Genet 15:3313–3323.
19. McIntosh AM, Moorhead TW, Job D, Lymer GK, Munoz Maniega S, McKirdy J, *et al*. (2008): The effects of a neuregulin 1 variant on white matter density and integrity. Mol Psychiatry 13:1054–1059.
20. Assaf Y, Alexander DC, Jones DK, Bizzi A, Behrens TE, Clark CA, *et al*. (2013): The CONNECT project: Combining macro- and microstructure. Neuroimage 80:273–282.
21. Zhang H, Schneider T, Wheeler-Kingshott CA, Alexander DC (2012): NODDI: Practical in vivo neurite orientation dispersion and density imaging of the human brain. Neuroimage 61:1000–1016.
22. Ye Z, Rae CL, Nombela C, Ham T, Rittman T, Jones PS, *et al*. (2016): Predicting beneficial effects of atomoxetine and citalopram on

response inhibition in Parkinson's disease with clinical and neuroimaging measures. Hum Brain Mapp 37:1026–1037.
23. Peruzzo D, Castellani U, Perlini C, Bellani M, Marinelli V, Rambaldelli G, *et al*. (2015): Classification of first-episode psychosis: A multimodal multi-feature approach integrating structural and diffusion imaging. J Neural Transm (Vienna) 122:897–905.
24. Yeomans D, Taylor M, Currie A, Whale R, Ford K, Fear C, *et al*. (2010): Resolution and remission in schizophrenia: Getting well and staying well. Adv PsychiatrTreat 16:86–95.
25. Leucht S, Samara M, Heres S, Patel MX, Woods SW, Davis JM (2014): Dose equivalents for second-generation antipsychotics: The minimum effective dose method. Schizophr Bull 40:314–326.
26. Rae CL, Correia MM, Altena E, Hughes LE, Barker RA, Rowe JB (2012): White matter pathology in Parkinson's disease: The effect of imaging protocol differences and relevance to executive function. Neuroimage 62:1675–1684.
27. Yendiki A, Koldewyn K, Kakunoori S, Kanwisher N, Fischl B (2014): Spurious group differences due to head motion in a diffusion MRI study. Neuroimage 88:79–90.
28. Smith SM, Jenkinson M, Johansen-Berg H, Rueckert D, Nichols TE, Mackay CE, *et al*. (2006): Tract-based spatial statistics: Voxelwise analysis of multi-subject diffusion data. Neuroimage 31:1487–1505.
29. Zhang H, Avants BB, Yushkevich PA, Woo JH, Wang S, McCluskey LF, *et al*. (2007): High-dimensional spatial normalization of diffusion tensor images improves the detection of white matter differences: An example study using amyotrophic lateral sclerosis. IEEE Trans Med Imaging 26:1585–1597.
30. Bach M, Laun FB, Leemans A, Tax CM, Biessels GJ, Stieltjes B, *et al*. (2014): Methodological considerations on tract-based spatial statistics (TBSS). Neuroimage 100C:358–369.
31. Tu S, Leyton CE, Hodges JR, Piguet O, Hornberger M (2015): Divergent longitudinal propagation of white matter degradation in logopenic and semantic variants of primary progressive aphasia. J Alzheimers Dis 49:853–861.
32. Keihaninejad S, Zhang H, Ryan NS, Malone IB, Modat M, Cardoso MJ, *et al*. (2013): An unbiased longitudinal analysis framework for tracking white matter changes using diffusion tensor imaging with application to Alzheimer's disease. Neuroimage 72:153–163.
33. Timmers I, Zhang H, Bastiani M, Jansma BM, Roebroeck A, Rubio-Gozalbo ME (2015): White matter microstructure pathology in classic galactosemia revealed by neurite orientation dispersion and density imaging. J Inherit Metab Dis, 38, 295–304.
34. Winkler AM, Ridgway GR, Webster MA, Smith SM, Nichols TE (2014): Permutation inference for the general linear model. Neuroimage 92: 381–397.
35. Winkler AM, Ridgway GR, Douaud G, Nichols TE, Smith SM (2016): Faster permutation inference in brain imaging. Neuroimage 141:502–516.
36. Smith SM, Nichols TE (2009): Threshold-free cluster enhancement: Addressing problems of smoothing, threshold dependence and localisation in cluster inference. Neuroimage 44:83–98.
37. Chang YS, Owen JP, Pojman NJ, Thieu T, Bukshpun P, Wakahiro ML, *et al*. (2015): White matter changes of neurite density and fiber orientation dispersion during human brain maturation. PloS One 10:e0123656.
38. Greenhill SD, Juczewski K, de Haan AM, Seaton G, Fox K, Hardingham NR (2015): NEURODEVELOPMENT. Adult cortical plasticity depends on an early postnatal critical period. Science 349:424–427.
39. Kodiweera C, Alexander AL, Harezlak J, McAllister TW, Wu YC (2016): Age effects and sex differences in human brain white matter of young to middle-aged adults: A DTI, NODDI, and q-space study. Neuroimage 128:180–192.
40. Cocchi L, Harding IH, Lord A, Pantelis C, Yucel M, Zalesky A (2014): Disruption of structure-function coupling in the schizophrenia connectome. Neuroimage Clin 4:779–787.
41. van den Heuvel MP, Fornito A (2014): Brain networks in schizophrenia. Neuropsychol Rev 24:32–48.
42. Fogelson N, Litvak V, Peled A, Fernandez-del-Olmo M, Friston K (2014): The functional anatomy of schizophrenia: A dynamic causal modeling study of predictive coding. Schizophr Res 158:204–212.
43. Adams RA, Stephan KE, Brown HR, Frith CD, Friston KJ (2013): The computational anatomy of psychosis. Front Psychiatry 4:47.
44. Corlett PR, Honey GD, Fletcher PC (2016): Prediction error, ketamine and psychosis: An updated model. J Psychopharmacol 30: 1145–1155.
45. Teufel C, Subramaniam N, Dobler V, Perez J, Finnemann J, Mehta PR, *et al*. (2015): Shift toward prior knowledge confers a perceptual advantage in early psychosis and psychosis-prone healthy individuals. Proc Natl Acad Sci U S A 112:13401–13406.
46. Cheung V, Chiu CP, Law CW, Cheung C, Hui CL, Chan KK, *et al*. (2011): Positive symptoms and white matter microstructure in never-medicated first episode schizophrenia. Psychol Med 41:1709–1719.
47. Dorph-Petersen KA, Pierri JN, Perel JM, Sun Z, Sampson AR, Lewis DA (2005): The influence of chronic exposure to antipsychotic medications on brain size before and after tissue fixation: A comparison of haloperidol and olanzapine in macaque monkeys. Neuropsychopharmacology 30:1649–1661.
48. Wang Q, Cheung C, Deng W, Li M, Huang C, Ma X, *et al*. (2013): White-matter microstructure in previously drug-naive patients with schizophrenia after 6 weeks of treatment. Psychol Med 43: 2301–2309.
49. Okugawa G, Nobuhara K, Takase K, Saito Y, Yoshimura M, Kinoshita T (2007): Olanzapine increases grey and white matter volumes in the caudate nucleus of patients with schizophrenia. Neuropsychobiology 55:43–46.
50. Boonstra G, van Haren NE, Schnack HG, Cahn W, Burger H, Boersma M, *et al*. (2011): Brain volume changes after withdrawal of atypical antipsychotics in patients with first-episode schizophrenia. J Clin Psychopharmacol 31:146–153.
51. Rokem A, Yeatman JD, Pestilli F, Kay KN, Mezer A, van der Walt S, *et al*. (2015): Evaluating the accuracy of diffusion MRI models in white matter. PloS One 10:e0123272.
52. Feinberg DA, Moeller S, Smith SM, Auerbach E, Ramanna S, Gunther M, *et al*. (2010): Multiplexed echo planar imaging for sub-second whole brain FMRI and fast diffusion imaging. PloS One 5:e15710.